AIP Conference Proceedings

Investigation of n-Al:ZnO/p-Cu_2O heterojunction for c-Si tandem heterojunction solar cell applications

Cite as: AIP Conference Proceedings **2147**, 130002 (2019); https://doi.org/10.1063/1.5123885
Published Online: 27 August 2019

Raj Kumar, Ørnulf Nordseth, Geraldo Cristian Vásquez, Sean Erik Foss, Eduard Monakhov, and Bengt Gunnar Svensson

ARTICLES YOU MAY BE INTERESTED IN

Efficiency improvement of bifacial PERC solar cell based on the optimization of rear structure
AIP Conference Proceedings **2147**, 110003 (2019); https://doi.org/10.1063/1.5123879

Inline deposited PassDop layers for rear side passivation and contacting of p-type c-Si PERL solar cells with high bifaciality
AIP Conference Proceedings **2147**, 110005 (2019); https://doi.org/10.1063/1.5123881

A facile way to improve the efficiency of perovskite/silicon four-terminal tandem solar cell based on the optimization of long-wavelength spectral response
AIP Conference Proceedings **2147**, 130003 (2019); https://doi.org/10.1063/1.5123886

Lock-in Amplifiers
Zurich Instruments
Watch the Video

AIP Publishing

© 2019 Author(s).

Investigation of n-Al:ZnO/p-Cu_2O Heterojunction for c-Si Tandem Heterojunction Solar Cell Applications

Raj Kumar[1,a)], Ørnulf Nordseth[2], Geraldo Cristian Vásquez[1], Sean Erik Foss[2], Eduard Monakhov[1], Bengt Gunnar Svensson[1]

[1]*Department of Physics/Center for Materials Science and Nanotechnology (SMN), University of Oslo, P. O. Box 1048, Blindern, NO-0316 Oslo, Norway*
[2]*Institute for Energy Technology (IFE), Department for Solar Energy, P.O. Box 40, NO-2027 Kjeller, Norway*

[a)]Corresponding author: raj.kumar@smn.uio.no

Abstract. In this work, an in-situ growth approach has been employed to fabricate Al:ZnO/Cu_2O/Cu and Al:ZnO/ZnO/Cu_2O/Cu heterojunctions using direct current (DC) and radio frequency (RF) magnetron sputtering technique in a controlled atmospheric condition. The effect of ZnO buffer layer thickness (30 and 50 nm) as well as in-situ Cu_2O annealing at 600 °C in low vacuum (~ 10^{-6} Torr) prior to Al:ZnO deposition were studied. The carrier density of Al:ZnO was ~ 2×10^{20} cm^3 with mobility ~ 8 cm^2/V·s and resistivity ~ 1×10^{-3} Ω·cm, while the carrier density of Cu_2O was 1×10^{15} cm^3 with mobility ~ 19 cm^2/V·s and resistivity ~ 200 Ω·cm. The heterojunctions were investigated by depth resolved Cathodoluminescence (CL) spectroscopy at 80 K to analyze the influence of defects at the interface. The two emissions at 1.51 eV (V_O^+) and 1.69 eV (V_O^{2+}) dominate in all CL spectra related to oxygen vacancy defects in Cu_2O. The relative intensity of the defect luminescence band V_O^+ respect to V_O^{2+} is greater at the interface compared to bulk Cu_2O, while the incorporation of the ZnO layer reduces significantly both radiative recombination and the V_O^{2+} related emission at the interface.

INTRODUCTION

Cuprous oxide (Cu_2O), being a semi-transparent binary oxide, economically cheap, abundant, non-toxic material with 'native' p-type conductivity, is a promising candidate as an absorber layer to realize heterojunctions with n-type materials, e.g., aluminum-doped zinc oxide (Al:ZnO or AZO) [1],[2]. Cu_2O has a direct energy bandgap (E_g) ~ 2.2 eV (at 300 K) with a strong absorption of photons with energies higher than E_g. Metal oxide heterojunctions and crystalline silicon-based solar cells have good potential for development of high performance tandem solar cells [3]. The AZO/Cu_2O heterojunction is a potential candidate material for tandem heterojunction solar cell configuration, i.e., a conventional c-Si bottom subcell is combined with an AZO/Cu_2O top subcell in a mechanical stack of independently connected cells [4-6]. The deposition of AZO/Cu_2O thin film stack on an optically transparent quartz substrate enables low-energy photons to be transmitted through the AZO/Cu_2O top subcell for subsequent absorption in the c-Si bottom subcell [7]. The maximum power conversion efficiency reported for an AZO/Cu_2O heterojunction solar cell is ~ 8.1% [8-10]. The theoretical efficiency of a thin film based tandem heterojunction solar cell is estimated about 30% depending upon the optical absorption, E_g, carrier transport, and luminescence efficiency of top cell [11], where estimated photon conversion efficiency range varied from 22% for a material with E_g ~1.5 eV to 16% for a material with E_g ~ 2.1 eV as a top subcell [12].

In this article, Cu_2O and AZO thin films were deposited by DC/RF magnetron sputtering technique without breaking the vacuum during the growth. This deposition process allows for controlling the growth conditions and parameters (Ar/O_2 ratio, substrate temperature, power, pressure) during the deposition. It will play a vital role to tailor the electronic/optical properties of the interface between different staking layers [13],[14]. In addition, a ZnO buffer layer was also incorporated between the AZO and Cu_2O layers with the aim to enhance the device

SiliconPV 2019, the 9th International Conference on Crystalline Silicon Photovoltaics
AIP Conf. Proc. 2147, 130002-1–130002-6; https://doi.org/10.1063/1.5123885
Published by AIP Publishing. 978-0-7354-1892-9/$30.00

performance by suppressing the formation of defects and improve the energy band alignment at the heterojunction interface.

EXPERIMENTAL METHOD

Various heterojunction thin film structures, including AZO/Cu_2O/Cu, AZO/Cu_2O (annealed at 600 °C in low vacuum ~ 10^{-6} Torr)/Cu, AZO/ZnO (30 nm)/Cu_2O/Cu and AZO/ZnO (50 nm)/Cu_2O/Cu were deposited by direct current/radio frequency (DC/RF) magnetron sputtering technique (Semicore Triaxis) on quartz substrates at 400 °C substrate temperature in a controlled environmental condition without breaking the vacuum (*in-situ* growth), in order to control the electronic properties of the heterojunction interface with better lattice match and to avoid any contamination during the process. The effect of *in-situ* Cu_2O annealing at 600 °C in low vacuum (~ 10^{-6} Torr) prior to AZO deposition were also investigated. The quartz substrates were cleaned in piranha and rinsed in deionized water. Subsequently, the substrates were blown dry with nitrogen and loaded into the deposition chamber. The Cu electrode (~ 500 nm) was deposited by DC sputtering from a 99.999% Cu target in Ar (50 sccm) with a substrate temperature of 400 °C after that Cu_2O (500 nm) was deposited by DC reactive sputtering in O_2/Ar ratio (7.5/42.5 sccm) at 400 °C. The target power was fixed at 100 W. The base pressure was kept below 5.0×10^{-7} Torr and the sample stage was rotated at a constant speed of 12 rpm during the deposition. The AZO (~ 200 nm) layer was deposited by RF sputtering (power 50 W) from an aluminum (2 wt %) doped ZnO target in Ar (50 sccm) at 400 °C. ZnO buffer layer (30 nm and 50 nm thickness) was deposited by RF sputtering (power 50 W) from ZnO target (99.99%) in Ar (50 sccm) at 400 °C after Cu_2O deposition.

Photolithography technique was used to deposit top metal contact. The aluminum (Al) contact (1 mm size and ~ 150 nm thickness) was deposited by e-beam evaporation onto the AZO surface at room temperature. The chemical etching with diluting HCl solution (5%) was employed to remove the selected area (~ 3 mm) of AZO/Cu_2O staking layers for edge isolation and to have Cu as back contact. The AZO and Cu_2O thin film thicknesses were determined to be ~ 200 nm and ~ 500 nm, respectively, by spectroscopic ellipsometry, while the Cu back contact of ~ 500 nm thickness was measured by stylus profilometer, showing good correlation with the thickness estimated from scanning electron microscope (SEM) imaging. The ZnO buffer layer thickness was estimated around ~ 30 nm and ~ 50 nm from the deposition rate. X-ray diffraction (XRD) patterns were acquired using a Bruker D8 Discover X-ray diffractometer with Cu Kα-radiation and a Bragg-Brentano configuration. Room temperature Hall effect measurements were conducted using the van-der Pauw method to determine the mobility, resistivity, and carrier density of AZO and Cu_2O films [15]. SEM was employed for cross section analysis of the heterojunction structure. Cathodoluminescence (CL) measurements were performed on all samples with a JEOL JSM-IT300 SEM equipped with a Delmic SPARC cathode-luminescence system. CL spectra were collected with an Andor Shamrock SR-193i spectrometer using a 500 l/mm grating and a charged coupled device (CCD) Andor Newton DU940P-BU2 detector. The CL measurements were carried out at 80 K with constant excitation power (1 μW) and e-beam energy from 3 to 20 keV in order to control the probing depth. All CL spectra have been calibrated for spectral shape and intensity in accordance to the measurements conditions.

RESULTS AND DISCUSSION

FIGURE 1a displays the AZO/Cu_2O/Cu heterojunction structure with 10 x 10 mm size with Cu (~3 mm) as back contact electrode and Al as top contact (1 mm size). **FIGURE 1**b shows the XRD patterns of the different heterojunction structures, while the inset of **FIGURE 1**b presents a SEM cross-section image of the AZO/Cu_2O/Cu heterojunction structure. The XRD peaks of the AZO (002), Cu_2O (111), Cu_2O (200), Cu (111), and Cu (200) crystalline orientations are shown in the 2θ scans, suggesting that the Cu_2O layer is polycrystalline with a dominating (111) orientation on Cu layer, while AZO deposited onto Cu_2O layer is dominating with (002) orientation, which shows the growth and orientation of different stacks on each other's during the device fabrication. The unwanted extra XRD peak like CuO was not observed which could have a detrimental effect on functional properties [15]. The carrier concentration, carrier mobility, and resistivity for AZO and Cu_2O (as-deposited) thin films on quartz, derived from Hall effect measurements at room temperature, are listed in **TABLE 1**. These values are comparable to those reported previously for sputter-deposited polycrystalline Cu_2O thin films on quartz [16].

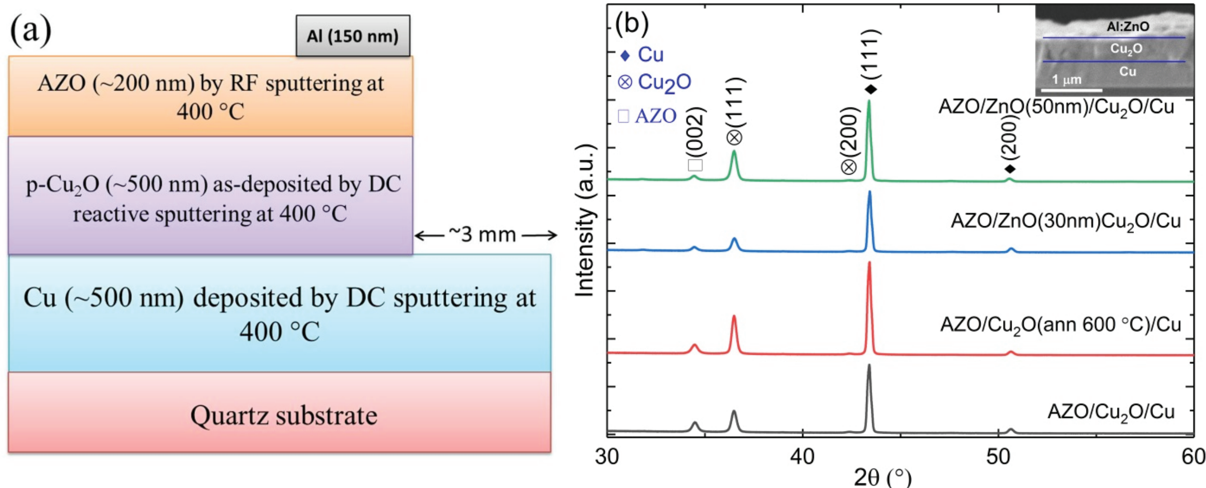

FIGURE 1. (a) Schematic illustration of the AZO/Cu_2O/Cu heterojunction structure and (b) XRD pattern of AZO/Cu_2O/Cu and various heterojunction devices, with the inset figure showing the cross-section SEM image of the AZO/Cu_2O/Cu heterojunction structure.

TABLE 1. Carrier concentration, mobility, and film resistivity for AZO and Cu_2O thin films on quartz are acquired using hall measurements at room temperature.

Material	Doping type	Carrier concentration [cm^{-3}]	Mobility [cm^2/V·s]	Resistivity [Ω·cm]
AZO	n	2×10^{20}	8	1×10^{-3}
Cu_2O	p	1×10^{15}	19	200

In multilayer heterojunction device, the lattice mismatch and interface among different layers play the critical roles which have a direct effect on the performance of the device. Various characterization techniques are available to investigate the heterojunction interface. I-V curves were measured at all devices to investigate the interface heterojunction. All devices show unstable rectifying behavior, likely due to lattice deformation, impurities or defects at the heterojunction interface. A stable rectifying junction is required to investigate the interface using other electrical techniques such as deep level transient spectroscopy (DLTS) and Thermal Admittance Spectroscopy (TAS). Therefore, an alternative technique, Cathodoluminescence (CL) has been employed. CL is a qualitative and non-destructive technique that can be used to investigate the radiative recombination of e-beam excited electrons from the different layers and interfaces of the heterojunction structure.

FIGURE 2 displays the CL spectra acquired at 80 K from AZO/Cu_2O/Cu heterojunction deposited at constant substrate temperature (**FIGURE 2**a), and a heterojunction growth with additional thermal annealing at 600 °C prior to AZO deposition (**FIGURE 2**b). The spectra were measured with e-beam energies of 3, 5, 10 and 20 keV. The depth of the generated carriers has been estimated by the e-beam energy deposition distribution shown in the inset of **FIGURE 2**b calculated by CASINO software [17]. The estimated depth profile where the injected electrons impinge their energy is around 60 nm, 150 nm, 400 nm, and higher than 700 nm for 3, 5, 10 and 20 keV, respectively. At the high energy side of the CL spectrum measured at 3 keV, a broad UV band can be identified at 3.5 eV assigned to the near band edge emission (NBE) from the AZO film [18], labelled as NBE (AZO) in **FIGURE 1**a. At lower energies, luminescence bands from the Cu_2O film can be observed as the excitonic yellow 1s emission (Y1: yellow line) at ~2 eV [19],[20] and two defect luminescence bands at 1.69 eV and 1.51 eV classically assigned to double (Vo^{2+}) and single ionized oxygen vacancies (Vo^{+}), respectively [21]. The observation of the Cu_2O related emissions reveals that generated carriers in the AZO layer move and recombine in the Cu_2O layer, or more likely near the AZO/Cu_2O interface. The broad and weak appearance of the Y1 emission can be due to the reduced grain size and polycrystalline nature of the as-deposited material. However, it is evident that the Cu_2O defect related states act as effective radiative recombination centres. At 5 keV, higher emission from deep defect levels in the AZO film known as the green emission band (GE) can be observed centred at ~2.3 eV near the Y1 emission, while the oxygen vacancy (Vo) related bands from Cu_2O only increase their total intensity without significant change in their intensity

ratio, peak positions or shape. The CL spectra measured at 10 and 20 keV show similar features. In both cases the luminescence from the Vo^{2+} related band from the Cu_2O layer dominates over the Vo^{+} defect band.

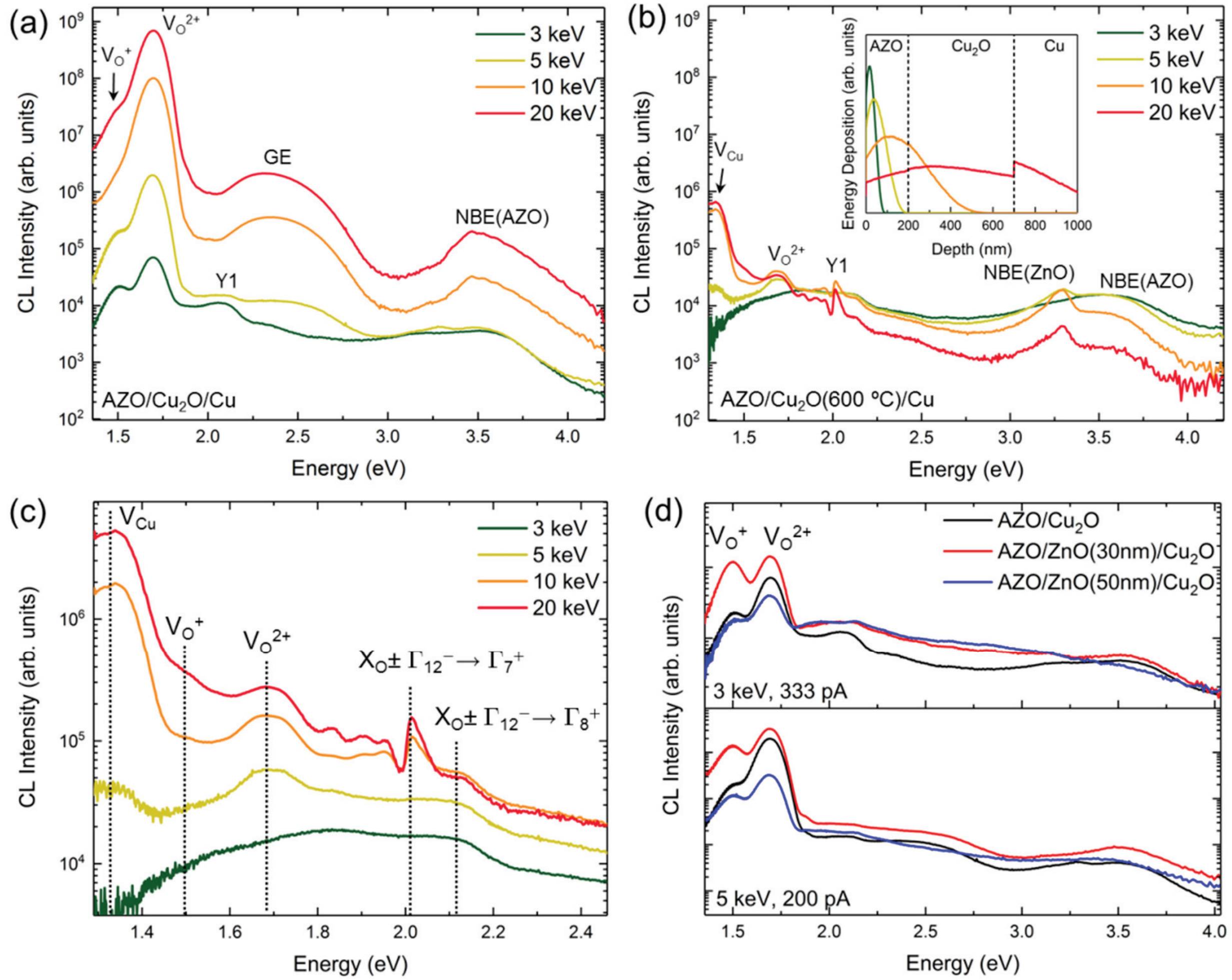

FIGURE 2. Cathodoluminescence (CL) spectrum measured at 80 K for (a) AZO/Cu_2O/Cu, and (b) AZO/Cu_2O (in-situ annealing during growth at 600 °C in low vacuum 10^{-6} Torr)/Cu. The inset in (b) presents the depth profile of the e-beam; (c) Extended region from 1.3 – 2.45 eV of figure (b); and (d) the CL spectra for AZO/Cu_2O, AZO/ZnO (30 nm)/Cu_2O and AZO/ZnO (50 nm)/Cu_2O heterojunctions.

The CL spectra of the sample annealed at 600 °C (*in-situ* in low vacuum 10^{-6} Torr) shown in **FIGURE 2**b are characterized by a total CL intensity decrease in both AZO and Cu_2O signals, that is likely due to increased non-radiative recombination channels despite the higher crystalline quality (**FIGURE 1**b). From the AZO layer it is important to note that a narrow band peaking at ~3.25 eV related to the ZnO NBE appears for e-beam energies >5 keV that is likely an indication of heterogeneous Al diffusion during film deposition. It may suggest that lower AZO temperature deposition is necessary in order to improve Al homogeneity. Regarding the Cu_2O luminescence, details of the spectral region from 1.3 to 2.45 eV has been enlarged in **FIGURE 2**c. At 3 keV the Cu_2O related emissions appear as a featureless band from 1.4 to 2.2 eV with a maximum at 1.83 eV and a shoulder at ~2.1 eV. The Vo^{2+} related band at 1.69 eV dominates the spectrum measured at 5 keV and a luminescence band assigned to Cu vacancies (V_{Cu}) [22] can be observed at ~1.34 eV. The Cu_2O related emissions change dramatically for 10 keV and 20 keV, corresponding to regions where carriers are generated and recombined in the Cu_2O layer according to the energy distribution shown in the inset of **FIGURE 2**b. In this case, the features of the Y1 excitonic emission can be resolved in the contributions from phonon-assisted transitions to the Γ^{7+} or Γ^{8+} valence bands assigned to orthoexcitons (XO) coupled with Γ^{12-} phonons [22], [23]. Additionally, the V_{Cu} defect band clearly dominates the CL spectrum while the Vo^{+} band at 1.5 eV is barely detectable. This result confirms that 3 and 5 keV measurements

yield the emission in the AZO layer and at the AZO/Cu_2O interface, while Cu_2O bulk emissions require that electrons penetrate and recombine radiatively in the Cu_2O layer.

Results from the as-deposited samples with a 30 nm and 50 nm ZnO intermediate (buffer) layer (AZO/ZnO (30 nm and 50 nm)/Cu_2O) are shown in the **FIGURE 2**d for 3 and 5 keV. Higher e-beam energies (10 keV and 20 keV) show characteristics similar to the sample in absence of the buffer layer. At 3 keV both samples show featureless CL signal in the spectral range from 2 keV, so mainly emissions from the Cu_2O defect bands can be detected. The AZO/ZnO (30 nm)/Cu_2O sample show an increased relative intensity of the Vo^+ defect band respect to Vo^{2+}, while the AZO/ZnO (50 nm)/Cu_2O sample show significantly weaker CL signal and Vo^+/Vo^{2+} intensity ratio similar to the AZO/Cu_2O sample. By increasing the e-beam energy to 5 keV the relative intensity associated to Vo^+ defects is higher on the samples in presence of the ZnO intermediate layer. It can be interpreted as a reduction of Vo^{2+} recombination at the ZnO/Cu_2O interface compared to AZO/Cu_2O. Additionally, by increasing the thickness of the ZnO intermediate layer the total luminescence emission is reduced by almost one order of magnitude, indicating that non-radiative recombination paths are favoured, which may imply an increase in the carrier lifetime at the interface [23].

SUMMARY

The heterojunction devices such as AZO/Cu_2O/Cu, AZO/Cu_2O (annealed at 600 °C in low vacuum ~ 10^{-6} Torr)/Cu, AZO/ZnO (30 nm)/Cu_2O/Cu and AZO/ZnO (50 nm)/Cu_2O/Cu were prepared by DC/RF sputtering, followed by photo-lithography and e-beam deposition, respectively. Cu_2O layer is polycrystalline with a dominating (111) orientation on Cu layer and AZO deposited onto Cu_2O layer is dominating with (002) orientation. The heterojunction devices were investigated by a non-destructive technique called CL. CL measurements at 80 K have been performed on all multilayer devices using different e-beam energies to enhance the signal from the heterojunction interface. Two emissions at 1.51 eV (V_O^+) and 1.69 eV (V_O^{2+}) dominate in all CL spectra measured on as-deposited samples related to V_O defects in Cu_2O. The V_O^{2+} luminescence is a very efficient recombination center in the Cu_2O layer and its intensity compete with V_O^+ at the interface. The enhancement in non-radiative recombination was observed on the samples with Cu_2O film annealed at 600 °C, characterized by lower total intensity and the presence of both V_O^{2+} emission and V_{Cu} defect band at the AZO/Cu_2O interface. In addition, lower temperature deposition of AZO might be necessary to avoid Al diffusion. The intermediate ZnO buffer layer reduces the total luminescence, and in greater extent the V_O^{2+} emission at the interface, which may indicate improvement of the carrier lifetime.

ACKNOWLEDGMENTS

This work was conducted under the research project “High-performance tandem hetero-junction solar cells for specific applications (SOLHET) http://solhet.eu/, financially supported by the Research Council of Norway (RCN), project number 251789, and the Executive Agency for Higher Education, Research Development and Innovation Funding (UEFISCDI) through the EU-H2020 M-Era.net program. The Research Council of Norway is acknowledged for the support to the Norwegian Micro- and Nano-Fabrication Facility, NorFab, project number 245963/F50, and FUNDAMeNT project (No. 251131). I would like to thank Mr. Viktor Bobal for technical support during the experiment.

REFERENCES

1. B. K. Meyer, A. Polity, D. Reppin, M. Becker, P. Hering, P. J. Klar, T. Sander, C. Reindl, J. Benz, M. Eickhoff, C. Heiliger, M. Heinemann, J. Bläsing, A. Krost, S. Shokovets, C. Müller, and C. Ronning, Phys. Status Solidi 249, 1487 (2012).
2. T. Minami, T. Hideki, S. Takahiro, M. Toshihiro and S. Hirotoshi, Japanese Journal of Applied Physics 43, no. 7A: L917 (2004).
3. D. V. Alexis, Journal of Physics D: Applied Physics 13, no. 5: 839 (1980).
4. Y. Takiguchi and S. Miyajima, Jpn. J. Appl. Phys. 54, 112303 (2015).
5. Ø. Nordseth, R. Kumar, K. Bergum, L. Fara, C. Dumitru, D. Craciunescu, F. Dragan, I. Chilibon, E. Monakhov, S. E. Foss, B. G. Svensson, Materials 11, 2593 (2018).

6. S. S. Wilson, J. P. Bosco, Y. Tolstova, D. O. Scanlon, G. W. Watson, H. A. Atwater, Energy Environ. Sci. 7, 3606 (2014).
7. Ø. Nordseth, R. Kumar, K. Bergum, L. Fara, S.E. Foss, H. Haug, F. Drăgan, D. Crăciunescu, P. Sterian, I. Chilibon, and C. Vasiliu, Green and Sustainable Chemistry, 7(01), pp.57-69 (2017).
8. T. Minami, Y. Nishi and T. Miyata, Appl. Phys. Express 9 052301 (2016).
9. Y. Nishi, T. Miyata and T. Minami, Journal of Vacuum Science & Technology A: Vacuum, Surfaces, and Films, 30(4), p.04D103 (2012).
10. A. E. Gunnæs, S. Gorantla, O. M. Løvvik, J. Gan, P. A. Carvalho, B. G. Svensson, E. V. Monakhov, K. Bergum, I. T. Jensen, and S. Diplas, The Journal of Physical Chemistry C 120, no. 41: 23552-23558 (2016).
11. P. T. White, L. N. Niraj and C. R. Kylie, IEEE Journal of Photovoltaics 4, no. 1: 208-214 (2014).
12. Y. Takiguchi and S. Miyajima, Japanese Journal of Applied Physics, 54 (11), p.112303 (2015).
13. Zubko, P., Gariglio, S., Gabay, M., Ghosez, P. and Triscone, J.M., Annu. Rev. Condens. Matter Phys., 2(1), pp.141-165 (2011).
14. Shahahmadi, S.A., Zulkefle, A.A., Hasan, A.K.M., Rana, S.M., Bais, B., Akhtaruzzaman, M., Alamoud, A.R.M. and Amin, N., 2016. Materials Science in Semiconductor Processing, 56, pp.160-165 (2016).
15. J. Gan, "Synthesis and Characterization of Cu_2O/ZnO Heterojunctions for Applications", PhD thesis, University of Oslo, 2017.
16. Y. S. Lee, M. T. Winkler, S. C. Siah, R. Brandt, T. Buonassisi, Applied Physics Letters 98, 192115 (2011).
17. D. Drouin, Microsc. Microanal. 12, 1512 (2006).
18. Q. Hou, F. Meng, and J. Sun, Nanoscale Res. Lett. 8, 144 (2013).
19. J. Li, Z. Mei, D. Ye, H. Liang, L. Liu, Y. Liu, A. Galeckas, A. Y. Kuznetsov, and X. Du, Opt. Mater. Express 3, 2072 (2013).
20. T. Tayagaki, A. Mysyrowicz, and M. Kuwata-Gonokami, J. Phys. Soc. Japan 74, 1423 (2005).
21. Y. Petroff, Y. Yu, and Y. R. Shen, Phys. Rev. B 12, 2488 (1975).
22. K. Bergum, H. N. Riise, S. Gorantla, P. F. Lindberg, I. J. T. Jensen, A. E. Gunæs, A. Galeckas, S. Diplas, B. G. Svensson, and E. Monakhov, J. Phys. Condens. Matter 30, 075702 (2018).
23. Frazer, L., Lenferink, E.J., Chang, K.B., Poeppelmeier, K.R., Stern, N.P. and Ketterson, J.B., Journal of Luminescence, 159, pp.294-302 (2015).